Published in final edited form as:

Mol Cell. 2019 June 20; 74(6): 1164–1174.e4. doi:10.1016/j.molcel.2019.04.008.

Crosstalk between RNA Pol II C-Terminal Domain Acetylation and Phosphorylation via RPRD Proteins

Ibraheem Ali[1,2], **Diego Garrido Ruiz**[3], **Zuyao Ni**[4], **Jeffrey R. Johnson**[1], **Heng Zhang**[6], **Pao-Chen Li**[1], **Mir M. Khalid**[1], **Ryan J. Conrad**[1,2], **Xinghua Guo**[4], **Jinrong Min**[6], **Jack Greenblatt**[4], **Matthew Jacobson**[3,5], **Nevan J. Krogan**[1,5], and **Melanie Ott**[1,2,7,*]

[1]J. David Gladstone Institutes, San Francisco, California, 94158, USA

[2]Department of Medicine, University of California San Francisco, San Francisco, California, 94143, USA

[3]Department of Pharmaceutical Chemistry, University of California San Francisco, San Francisco, California, 94143, USA

[4]Donnelly Centre, University of Toronto, Toronto, Ontario, Canada

[5]California Institute for Quantitative Biosciences (QBC) at UCSF, San Francisco, California, 94143, USA

[6]Structural Genomics Consortium, University of Toronto, Ontario, Canada

[7]Lead Contact

SUMMARY

Post-translational modifications of the RNA polymerase II C-terminal domain (CTD) coordinate the transcription cycle. Crosstalk between different modifications is poorly understood. Here, we show how acetylation of lysine residues at position 7 of characteristic heptad repeats (K7ac)—only found in higher eukaryotes—regulates phosphorylation of serines at position 5 (S5p), a conserved mark of polymerases initiating transcription. We identified the regulator of pre-mRNA domain-containing (RPRD) proteins as reader proteins of K7ac. K7ac enhanced CTD peptide binding to the CTD-interacting domain (CID) of RPRD1A and RPRD1B proteins in isothermal calorimetry and molecular modeling experiments. Deacetylase inhibitors increased K7ac- and decreased S5-phosphorylated polymerases, consistent with acetylation-dependent S5 dephosphorylation by an RPRD-associated S5 phosphatase. Consistent with this model, RPRD1B

*Correspondence: melanie.ott@gladstone.ucsf.edu.

AUTHOR CONTRIBUTIONS

I.A. designed the study, validated SILAC hits, conducted KDACi experiments, western blotting and quantification with assistance from M.K., performed ChIP-qPCR and ChIP-seq experiments and analyses, performed knockdown experiments, RNA-seq, and statistical analyses. P.C.L. and J.J. performed SILAC experiments and mass-spectrometric data analysis. Z.N., H.Z., and X.G. performed ITC experiments. D.G.R. performed molecular modeling experiments. R.J.C. supported ChIP-seq analysis. J.G., J.M., M.J., and N.K. supervised experiments. M.O. supervised the study design and data collection. I.A. and M.O. wrote the manuscript.

DECLARATION OF INTERESTS

The authors declare no competing interests.

knockdown increased S5p, but enhanced K7ac, indicating RPRD proteins recruit K7 deacetylases, including HDAC1. We also report auto-regulatory crosstalk between K7ac and S5p via RPRD proteins and their interactions with acetyl- and phospho-eraser proteins.

Graphical Abstract

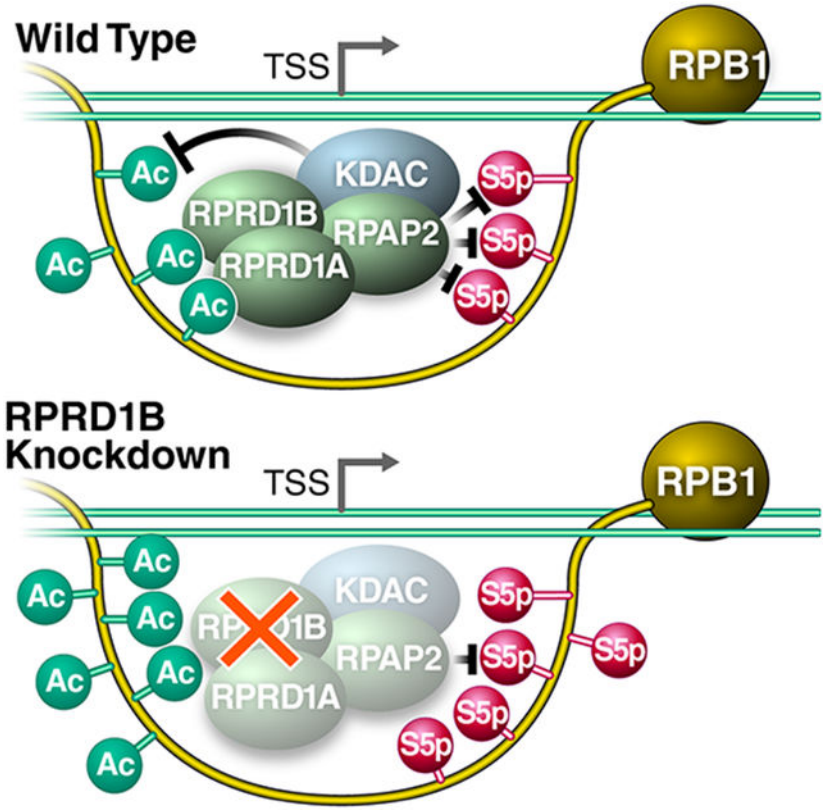

eTOC Blurb

Ali et al. (2019) uncover an intricate interplay between RNA Pol II CTD K7-acetylation and S5-phopshorylation in mammalian cells that is regulated by RPRD proteins. This finding highlights a mechnism which regulates the transition into transcription elongation that is unique to vertebrates.

Keywords

post-translational modification; transcription; phosphorylation; acetylation; crosstalk; histone deacetylase; polymerase; gene regulation

INTRODUCTION

The RNA polymerase II (Pol II) complex is highly conserved in all eukaryotic cells and responsible for production of most gene expression products (Eick and Geyer, 2013, Buratowski, 2003, Harlen and Churchman, 2017). RPB1, the largest subunit of the complex, contains the catalytic core of the complex and a unique regulatory region called the C-terminal domain (CTD). In eukaryotes, the CTD is composed of 20 or more repeats with a

heptad consensus sequence, $Y_1S_2P_3T_4S_5P_6S_7$, which is highly conserved from yeast to humans. In multicellular eukaryotes, the CTD is expanded and contains a varying number of non-consensus repeats, depending on the organism (Chapman et al., 2008). The 52 repeats of the mammalian CTD can be divided into 21 mostly consensus repeats proximal to the enzymatic core, and 31 non-consensus repeats distal from the core with less fidelity to the consensus. Divergence from the consensus sequence most commonly occurs at position 7, where the consensus serine is most commonly replaced with an asparagine (N), threonine (T), or lysine (K) (Eick and Geyer, 2013, Hsin and Manley, 2012, Harlen and Churchman, 2017). The CTD is intrinsically disordered and functions as an interaction platform for accessory proteins required for transcription and transcription-associated RNA-processing events (Jasnovidova and Stefl, 2013, Buratowski, 2009, Hsin and Manley, 2012, Zaborowska et al., 2016).

The heptad repeats within the CTD are extensively and dynamically post-translationally modified at different times during the transcription cycle. Of the seven consensus CTD residues, five can be phosphorylated (Y1, S2, T4, S5, and S7), and the two remaining proline residues can undergo isomerization to *cis* or *trans* conformations (Heidemann et al., 2013, Yurko and Manley, 2018). Serine-5 phosphorylation (S5p) and serine-2 phosphorylation (S2p) are the most thoroughly studied CTD modifications (Jasnovidova and Stefl, 2013, Buratowski, 2009, Harlen and Churchman, 2017). Serine-5 is phosphorylated by the cyclin-dependent kinase 7 (CDK7) subunit of general transcription factor TFIIH, is enriched at promoters, and decreases successively towards the 3′ end of genes (Ebmeier et al., 2017, Brookes et al., 2012). The phosphorylated serine-2 mark, placed by several kinases (CDK9, CDK12, CDK13 and BRD4), starts to accumulate downstream of transcription start sites and steadily increases towards the 3′ ends of genes, reflecting its critical role in productive polymerase elongation (Bartkowiak et al., 2010, Devaiah et al., 2012, Nechaev and Adelman, 2011). Similar to S5p, Serine-7 phosphorylation (S7p) is catalyzed by CDK7, is enriched near promoters and in gene bodies, and regulates the expression snRNA genes (Brookes et al., 2012, Egloff et al., 2012). Tyrosine-1 phosphorylation is enriched near promoters, and has been linked to enhancer and antisense transcription, as well as transcription termination (Descostes et al., 2014, Shah et al., 2018). Threonine-4 phosphorylation is enriched in coding regions and is required for cell viability and transcription elongation (Hintermair et al., 2012).

Post-translational modifications (PTMs) specifically found in non-consensus repeats include asymmetric dimethylation of a single arginine (R1810me2), conserved among some metazoa, that regulates transcription of small nuclear and nucleolar RNAs (Sims et al., 2011). In addition, lysine residues at position 7 of eight heptad repeats are acetylated by the acetyltransferase p300/CBP (KAT3A/B) (K7ac), and are also mono- and di-methylated by an as-yet-unknown methyltransferase (Voss et al., 2015, Schroder et al., 2013, Dias et al., 2015, Weinert et al., 2018). These lysine residues evolved in higher eukaryotes in the common ancestor of the metazoan lineage, and are highly conserved among vertebrates (Simonti et al., 2015). While lysine-7 mono- and di-methylation marks are found near promoters, K7ac is enriched in gene bodies (Dias et al., 2015). K7 residues are required for productive transcription elongation of immediate early genes in response to epidermal growth factor stimulation (Schroder et al., 2013). Importantly, K7ac marks are found at

~80% of actively transcribed genes, with a peak in signal +500 bp downstream of the transcription start site (TSS), indicating that the modification could more broadly regulate the transition from transcription initiation to productive elongation (Schroder et al., 2013). In a genetic model in which all eight K7 residues were mutated to arginines (8KR), cells expressing 8KR RPB1 exhibited altered expression of genes relating to development, multicellularity and cell adhesion, underscoring a critical role of K7ac in the development of higher eukaryotes (Simonti et al., 2015).

Effector proteins interacting with differentially modified CTDs often contain a so-called CTD-interacting domain (CID), which is one of the best-studied CTD-binding modules and is conserved from yeast to humans (Ni et al., 2011). The mammalian Regulator of Pre-mRNA Domain-containing (RPRD) proteins 1A, 1B and RPRD2 proteins are homologues of the yeast transcription termination factor *Rtt103*, and each contains a CID (Ni et al., 2011). *Rtt103* and RPRD CIDs bind CTD peptides carrying S2p, but not S5p; S7p and unmodified K7 residues reside at the edge of the CID binding cleft, and can be substituted without altering their binding affinity (Ni et al., 2014, Meinhart and Cramer, 2004, Jasnovidova et al., 2017). RPRD1A and RPRD1B are found in macromolecular complexes that associate with Pol II and transcription regulatory factors, including the S5-phosphatase RPAP2 (Ni et al., 2011, Ni et al., 2014, Morales et al., 2014, Patidar et al., 2016, Liu et al., 2015). RPRD1A, also called P15RS, regulates G1/S cell-cycle progression and suppresses Wnt and β-catenin signaling via interactions with the class I lysine deacetylase HDAC2 and transcription factor 4 (TCF4) (Wu et al., 2010, Liu et al., 2015, Jin et al., 2018, Liu et al., 2002). RPRD1B, also called CREPT, was identified in a mass spectrometry (MS)-based screen for mammalian Pol II-interacting proteins; it is upregulated in various cancers and regulates genome stability and transcription termination (Lu et al., 2012, Zhang et al., 2018, Morales et al., 2014, Patidar et al., 2016). Although the homology with *Rtt103* implies a conserved role in transcription termination and explains why the proteins are enriched in the 3′ ends of eukaryotic genes, an additional less well-defined role of RPRD proteins has emerged at the 5′ ends of genes in higher eukaryotes. This involves a mechanism to regulate genome stability through the resolution of R-Loops, which are DNA-RNA hybrids (Lu et al., 2012) as well as the recruitment of RPAP2 to initiating RNA Pol II (Ni et al., 2014).

In this study, we provide molecular insight into the role of RPRD proteins at the 5′ ends of genes and connect RPRD proteins with K7ac. We find that RPRD proteins via their CIDs specifically interact with K7ac, and that this interaction promotes S5-dephosphorylation at and beyond +500 bp downstream of the TSS. These data support a model in which vertebrates evolved specific crosstalk between S5p and K7ac to ensure precise transcription initiation dynamics and a timely transition to a productive elongation phase at a defined distance from the TSS.

RESULTS

Preferential Binding of RPRD Proteins to Acetylated RPB1

To identify proteins that interact with Pol II K7ac, we performed stable isotope labeling with amino acids in cell culture (SILAC). We overexpressed HA-tagged RPB1 proteins, either wild type (WT) or 8KR mutant, in HEK293T cells. The proteins also contained a known α-

amanitin resistance mutation enabling propagation of successfully transfected cells in the presence of α-amanitin, which induces the degradation of endogenous Pol II (Bartolomei and Corden, 1987). After culture of cells in differential metabolic labeling medium, RPB1-containing complexes were purified via their HA tag and subjected to MS analysis (Figure 1A, Supplemental Table 1). We found all members of the RPRD family preferentially bound to WT RBP1, including RPRD1A, RPRD1B, RPRD2 along with several of their interacting partners, such as RPAP2, RPAP3, MCM7 and RUVB1, that were identified by MS (Ni et al., 2011, Patidar et al., 2016) (Figure 1B).

Using HA-immunopurification and western blotting, we confirmed enrichment of K7ac ($p = 0.014$) and RPRD1B ($p=0.0098$) in WT relative to 8KR samples, the most thoroughly studied of the RPRD family (Figure 1C). In addition, we confirmed that the RPRD-interacting protein RPAP3 ($p = 0.049$), binds preferentially WT RPB1 protein relative to the 8KR mutant. However, HSP90, another hit in the screen, showed no preferential interaction in follow-up studies (Figure 1C, D). The enrichment of endogenous RPRD1B and RPAP3 proteins after immunoprecipitation of WT, but not mutant, HA-RPB1 was consistent among three or more independent experiments and statistically significant (Figure 1D). We also tested the interaction of endogenous RPB1, RPRD1A and RPRD1B proteins in NIH3T3 cells treated with lysine deacetylase (KDAC) inhibitors. KDAC inhibitor treatment induced robust hyperacetylation of endogenous RPB1 in input material as tested with an antibody specific for K7ac (Schroder et al., 2013), but did not change total Pol II protein levels as measured with the H224 antibody (Figure 1E). After pulldown of endogenous Pol II, more RPRD1A and RPRD1B proteins were recovered when cells were treated with KDAC inhibitors as compared to vehicle-treated cells, confirming positive regulation of the RPB1:RPRD interaction by acetylation (Figure 1E, F).

Next, we tested *in vivo* recruitment of RPRD1B to a known target gene, *Leo1* (Ni et al., 2011). Using chromatin immunoprecipitation (ChIP) followed by quantitative PCR, we found RPRD1B recruitment to the *Leo1* promoter (+33 bp) consistently enhanced in NIH3T3 cells treated with KDAC inhibitors as compared to vehicle-treated cells (Figure 1G). Similar to what we observed by western blotting, K7 residues were hyperacetylated at the Leo1 promoter in response to KDAC inhibition in ChIP analysis with the K7ac-specific antibody. Importantly, Pol II occupancy as measured with the 8WG16 antibody, which correlate with total Pol II levels (Vian et al., 2018, Tsai et al., 2018), did not increase under KDAC inhibition, confirming K7 hyperacetylation and enhanced RPRD1B recruitment in response to KDAC inhibition (Figure 1G).

Direct Interaction of K7ac with RPRD CTD-Interacting Domains

To test whether K7ac modulates CTD-interacting domain (CID) binding to RPRD CIDs, we performed isothermal titration calorimetry (ITC) to measure the binding free energy between synthetic CTD peptides and purified CID domains from both RPRD1A and RPRD1B proteins. We generated CTD peptides spanning ~3 heptad repeats (20 amino acids) with repeat 39 at the center. This region was chosen because it is acetylated and phosphorylated *in vivo* (Voss et al., 2015, Weinert et al., 2018), and contains multiple consecutive K7 residues (Figure 2A). Peptides were synthesized in an unmodified, acetylated (K7ac), or

phosphorylated (S2p and S5p) state. S2p was included as a positive control as it enhances CTD:CID interactions, while S5p served as a negative control (Ni et al., 2014, Pineda et al., 2015). In addition, we combined S2p and S5p with K7ac to investigate potential combined effects. Compared to the unmodified CTD, binding of the RPRD CIDs to CTD peptides carrying K7ac had a significantly lower K_d (2.3-fold reduction for RPRD1A and 3.8-fold for RPRD1B), indicating enhanced binding (Figures 2B–E). S2p itself had a robust effect in enhancing CID binding, as previously observed, but combining K7ac with S2p further decreased the K_d by 2.8-fold and 4.2-fold, respectively. S5p-carrying peptides did not interact with CID proteins as expected, and adding K7ac did not further enhance binding (Figures 2B–E). These observations indicate that K7ac enhances the interaction of RPRD proteins with the Pol II CTD with and without additional S2p marks.

Molecular Modeling of K7-Acetylated CTD Peptides with CID Domains

To better understand the mechanism for how K7ac stabilizes the binding of the CID and CTD peptides, we performed molecular modeling with published RPRD1B CID structures bound to CTD peptides [pdb: 4Q94 (dimer) and 4Q96 (tetramer)]. RPRD protein dimerization is believed to occur through coiled-coil domain interactions that are not present in these structures (Mei et al., 2014, Ni et al., 2014), which nonetheless dimerize and tetramerize by domain swapping. We proceeded with *in silico* analyses of both structures and searched for consistencies between them. Because phosphorylation and acetylation change the net charge of the peptide fragment, we first calculated the electrostatic potential of the CID structure to understand the charge distribution along the binding cleft (Dolinsky et al., 2004). We found that the recognition module within the CID in the dimeric and tetrameric structures has a positively charged binding pocket with numerous amide-containing residues within 5Å of the peptide (Figures 3A–D, Figure S1A–D). Acetylation and thus charge neutralization of the CTD lysine side chain favors interaction with this binding pocket by reducing electrostatic repulsion with the positively charged RPRD domains.

We also obtained 20-ns molecular dynamics trajectories to refine the models and identify residues within the CID that directly interact with S2p and K7ac and, thus, contribute to the recognition of these PTMs. Through these simulations, we reproduced the reported coordination between S2p and R106 (Ni et al., 2014), and observed that the two K7 residues in the acetylated state formed transient interactions with nearby CID residues (Figure 3C, D). In particular, the first acetylated K7 residue in the CTD peptide formed transient hydrogen bonds with two spatially proximal CID residues (N18 and N54). The second acetylated K7 residue interacted with CID residues at the other end of the binding cleft (Q24, Q68, N69 and R72) (Figure 3C, D). Similar results were obtained in simulations of the tetrameric structure, which also showed coordination between S2p and R106 along with similar transient hydrogen-bonding between K7ac and several residues in the CID (N18, Q20, E92 and K96) (Figure S1E, F). These results suggest that the acetylated lysine forms transient hydrogen bonding interactions that may contribute to binding stability, particularly with asparagine and glutamine that, like acetylated lysine, contain an amide group in the side chain.

Based on these observations, we hypothesized that RPRD1B evolved to specifically recognize K7ac through spatially proximal amide-containing side chains. Specific modes of recognition evolved to interact with different combinations of CTD modifications (Becker et al., 2008, Ni et al., 2014). For example, the SCAF8 protein recognizes doubly phosphorylated CTD peptides at S5 and S2 to regulate a putative role in pre-mRNA processing (Becker et al., 2008, Patturajan et al., 1998). Sequence alignment of CID domains reveals that RPRD proteins contain conserved asparagine and glutamine residues at key positions near the CID binding cleft. In contrast, the corresponding residues of SCAF family CID domains contain lysine, arginine or histidine residues (Figure 3I). We performed molecular modeling with acetylated non-consensus peptides that interact with the SCAF8 crystal structure (PDB: 3D9K). Interestingly, the SCAF8 CID binding interface contains a stronger net positive charge relative to RPRD1B with several lysine, arginine and histidine residues less than 5Å from the CTD peptide (Figure 3E, F). Only two amide-containing side chains were observed in the binding region (Q72, N120) compared with nine residues observed in RPRD1B (Figure 3G, H). These data indicate K7 acetylation interacts with amide groups in stabilizing CID-CTD interactions in RPRD proteins, something not conserved across other CID containing proteins (Figure 3I).

Increased K7ac Correlates with Reduced S5p Downstream of Transcription Start Sites

RPDR1 proteins interact with RPAP2, the mammalian homolog of yeast *Rtr1* and a known S5 phosphatase (Ni et al., 2011). We tested the influence of K7ac on S5p levels by performing ChIP-seq with antibodies specific for K7ac, S5p (4H8) and unmodified (8WG16) Pol II in chromatin isolated from NIH3T3 cells treated with KDAC inhibitors. Average metagene profiles measured as reads per million, relative to input controls, were generated for all expressed genes (Ramirez et al., 2016) (Figure 4A–C). KDAC inhibition increased genome-wide Pol II-K7ac occupancy as expected, particularly ≥500 bp downstream of the TSS within the gene body and downstream thereof. Pol II occupancy as measured with the 8WG16 antibody was not markedly changed by KDAC inhibition (Figure 4A, B). Interestingly, S5p levels around the TSS remained unchanged, while beyond the ≥500 bp mark S5p levels decreased below the level of control cells, mirroring enhanced K7ac (Figure 4C). These data confirm that Kac and S5p levels are inversely correlated with a control point ≥500 bp downstream of the TSS.

A focused analysis of known target genes of RPRD1B, such as *Leo1* and *Cyclin D1* (Lu et al., 2012, Ni et al., 2011), showed corresponding profiles with lowered S5p and enhanced K7ac levels downstream of the TSS in response to KDAC inhibition (Figure 4D). But for ~10% of actively expressed genes, including *Tub1a1* and *Mdm2*, S5p was not downregulated in response to KDAC inhibition despite strong upregulation of K7ac. These results indicate that these genes are possibly controlled by mechanisms other than the RPRD proteins (Figure 4E). Unfortunately, we could not examine the occupancy of RPRD proteins genome-wide as the available antibodies had an insufficient signal-to-noise ratio in ChIP-seq experiments (data not shown).

RPRD1B Knockdown Perturbs Both K7ac and S5p Marks Genome-Wide

Overexpression of RPRD proteins decreases S5p levels at the *Leo1* gene. This finding is consistent with a model in which RPRD proteins recruit the S5 phosphatase RPAP2 (Ni et al., 2011). We now performed the inverse experiment and knocked down RPRD1B in NIH3T3 cells using lentiviral shRNAs. A 50% knockdown efficiency was sufficient to induce global S5 hyperphosphorylation as observed by western blotting, indicating a critical role of RPRD1B in overall S5 dephosphorylation. Surprisingly, we also observed a consistent upregulation of K7ac levels in RPRD1B knockdown cells, suggesting a K7 deacetylase was recruited by RPRD proteins in addition to the S5 phosphatase (Figure 5A). No change in Pol II levels as measured with the H-224 antibody was observed. Marked S5 hyperphosphorylation was also observed when the HA-8KR mutant RPB1 protein was immunoprecipitated from transfected NIH3T3 cells, confirming that K7 residues are required for proper S5 dephosphorylation (Figure 5B). In addition, we found endogenous HDAC1 protein co-immunoprecipitating with endogenous RPRD1B proteins in NIH3T3 cells, pointing to HDAC1 as a specific RPRD1-associated K7 deacetylase (Figure 5C).

Next, we performed ChIP-seq in RPRD1B knockdown cells with antibodies against K7ac, S5p and unmodified Pol II. The most striking finding was the induction of a distinct TSS-proximal increase in K7 acetylation with minimal changes to 8WG16 Pol II occupancy (Figure 5D and 5E). This is consistent with the observation that K7ac was induced upon RPRD1B knockdown in western blot experiments (Figure 5A) and underscores a model where RPRD1B recruits a K7 deacetylase that counterbalances K7 acetylation within the first 500–1000 bp of transcribed genes. In conjunction with this, a dramatic increase in S5p upon RPRD1B knockdown (Figure 5D, F) fits well with the observation that reduced RPRD1B levels globally induce S5 hyperphosphorylation due to the lack of S5 phosphatase recruitment. Interestingly, K7ac enrichment was localized specifically to the TSS-proximal region, whereas S5p levels were higher globally than in cells treated with control shRNAs.

RNA-seq on RPRD1B knockdown cells identified 271 differentially expressed genes as compared to control shRNA-treated cells (Figure S2A, Table S2). RPRD1B was among the most significantly downregulated genes with an mRNA knockdown efficiency of 41% ($p = 0.0019$; Figure S2D), similar to what was observed for protein expression. Gene Ontology analysis on dysregulated genes indicated that RPRD1B knockdown induced changes in genes related to developmental processes, multicellular organismal development and cell adhesion, consistent with previous findings that complete knockout of the factor causes embryonic lethality (Morales et al., 2014) (Figure S2B–D). This finding agrees with studies indicating that K7ac specifically evolved in higher eukaryotes and regulates developmental genes with significant enrichment for evolutionary origins in the early history of eukaryotes through early vertebrates (Simonti et al., 2015, Schroder et al., 2013). These data identify RPRD1B as a regulator of genes involved in multicellular organismal development and further support the model that RPRD proteins are relevant reader proteins of the K7ac mark in higher eukaryotes.

DISCUSSION

In this study, we report a molecular function for K7ac in decreasing S5p levels in the transition from transcription initiation to elongation. We show that K7ac enhances the recruitment of RPRD proteins to the initiated Pol II complex to facilitate S5 dephosphorylation; this occurs presumably via RPAP2, their interacting S5 phosphatase (Figure 6A). Surprisingly, we found that lack of RPRD1B protein expression also increased K7ac levels, indicating that in addition to binding an S5 phosphatase, RPRD proteins recruit a K7 deacetylase that we identified as HDAC1. This provides a unique autoregulatory mechanism as binding to RPRD proteins to K7ac ultimately leads to the removal of the mark. Previous studies highlighted the importance of S2p in enhancing the interaction between the CTD and RPRD CID domains (Ni et al., 2014, Pineda et al., 2015), and so, the emergence of S2p downstream of K7ac may serve to maintain RPRD recruitment to complete S5 dephosphorylation during the early phase of transcription elongation (Ni et al., 2014). When levels of K7ac were perturbed by KDAC inhibitor treatment (Figure 6B) or RPRD1B knockdown (Figure 6C), recruitment of the S5 phosphatase was either enhanced, resulting in increased S5 dephosphorylation and lower S5p levels genome-wide, or recruitment was diminished, enhancing S5p levels, respectively. Therefore, these data support a model in which dynamics of K7 acetylation evolved to blunt the peak of S5 phosphorylation at a precise distance from the TSS in higher eukaryotes, likely facilitating the transition between transcription initiation and productive elongation.

We previously reported a transient enrichment in the occupancy of K7-acetylated Pol II located approximately +500 bp downstream of the TSS when we normalized K7ac peaks to unmodified Pol II occupancy on expressed genes (Schroder et al., 2013). This fits well with the self-limiting nature of K7ac where the modification recruits HDAC1 to support a negative feedback loop of K7ac via the RPRD reader proteins. Here we observed characteristic changes in S5p levels at and beyond the +500 bp mark that support the model that K7ac and S5p are regulated by RPRD proteins. In our current study, peaks proximal to the +500 bp mark behaved on average differently than peaks at or beyond the mark. There are several possible explanations. A) RPRD proteins are recruited specifically to the +500 bp location (at the peak of K7ac) and exert their effect on S5p and K7ac in this region and beyond. B) The balance between S5 phosphorylation and dephosphorylation immediately downstream of the TSS is shifted towards S5p, and efficient dephosphorylation only occurs after CDK7 levels are additionally lowered beyond the TSS (Ebmeier et al., 2017). C) The transition of Pol II into elongation and the occurrence of S2p at the transition point allow efficient RPRD association and S5 dephosphorylation and K7 deacetylation. We envision that multiple of the mechanisms could be in place to explain the observed changes.

An important finding of our study is that K7ac enhances the binding of the RPRD CIDs to CTD peptides. We show that the affinity of the CID:K7ac interaction is ~90 μM, which lies in the range of acetyl-lysine interactions with bromodomains, the latter being the “classical” Kac recognition domain (Muller et al., 2011). Interestingly, the K7ac:CID interaction accommodates additional phosphorylation marks, such as S2p. This supports previous findings that the CID domain creates a positively charged “channel” in which the CTD peptide is bound, depending on its PTM status (Jasnovidova et al., 2017, Ni et al., 2014).

Molecular modeling suggests that K7ac recognition occurs through electrostatic interactions and hydrogen bonding with various residues of the CID. The principles of specific recognition of phosphorylated amino acids have been well-studied and are consistent with the features we highlighted for S2p.

Although lysine acetylation has received less attention, our results suggest that side chains containing amide groups (N and Q) are important and form transient hydrogen bonds with the amide group of acetylated K7 residues. The amide groups in proteins, including those in the backbone and asparagine and glutamine side chains, tend to interact with each other, such as in secondary structure elements, asparagine capping the N-terminal end of alpha helices, and poly-glutamine repeats (Perutz et al., 1994). It is especially interesting that N18, N69 and Q24, which form hydrogen bonds with the acetylated lysine amide in the dimer or tetramer models, are conserved across RPRD proteins in mammals (Ni et al., 2014), but not in other CTD-binding proteins, such as SCAF8. Furthermore, we note that several CTD heptad repeats contain asparagine at position 7. We speculate that RPRD proteins may recognize such repeats, although this will require further experiments.

Serine-7 phosphorylation is the third-best studied PTM of the CTD. In mammals, S7p is enriched with S5p near promoters, but is uniquely stable in gene bodies (Descostes et al., 2014). Similar to K7ac, S7-phosphorylated residues are considered docking stations for RPAP2 that regulate S5-dephosphorylation and expression of snRNA genes (Egloff et al., 2012). Interestingly, S7p also enhances CTD:CID interaction consistent with the enhancement of electrostatic stability we describe here for K7ac (Egloff et al., 2012, Ni et al., 2014). Recent studies examined individual repeat PTMs *in vivo* and showed that CTD heptads are generally phosphorylated at one position per repeat (Schuller et al., 2016, Suh et al., 2016). This supports a model of dynamic movement along the 52 mammalian CTD repeats proposed here where the RPRD complex may start at distal non-consensus regions and work its way up to more proximal consensus regions to reach all S5p marks and allow maximal placement of S2p.

Another notable finding is the autoregulatory nature of K7ac. Although RPAP2 is a known S5 phosphatase, we showed that HDAC1 is an RPRD1B-associated deacetylase. Previous studies with overexpressed proteins identified HDAC2 as a RPRD1A-associated deacetylase and, thus, another possible candidate for CTD regulation (Liu et al., 2015). However, using endogenous proteins, we found no HDAC2 associated with RPRD proteins, but this may be due to limited sensitivity of the antibodies used (data not shown). The two candidates, HDAC1 and HDAC2, are consistent with our previous observations that class I/II KDACs are involved in deacetylation of the hypophosphorylated form of Pol II during or after transcription initiation (Schroder et al., 2013). Notably, HDAC1 and HDAC2 often function together within the NuRD complex, and further studies will investigate how NuRD complex proteins could regulate K7ac and thus Pol II-dependent transcription (Xue et al., 1998, Basta and Rauchman, 2015).

Gene expression changes as a consequence of RPRD1B knockdown were moderate, but the cellular pathways altered in response to RPRD1B knockdown revealed a relevant list of genes. These were mainly involved in development of multicellular organisms and were

strikingly similar to differentially regulated pathways found in WT and 8KR-Pol II expressing cells (Simonti et al., 2015). We have previously shown that K7ac evolution in higher eukaryotes presented a unique mode by which transcription elongation is regulated in mammals. We propose that the regulation of K7ac is linked to the now reported recruitment of RPRD proteins and the corresponding S5 dephosphorylation, a step tightly controlled in its dynamics in yeast. The question of why the need arose to control S5p with K7ac in multicellular organisms at a defined distance from the TSS remains unanswered but will be further examined. At this point, our data underscore a key role of controlled CTD PTM regulation at the transition from initiation to elongation important for the expression of developmentally relevant genes; they further demonstrate that this control depends on precise interactions with the RPRD complex, which performs reader and effector functions at a well-defined time during the transcription cycle.

STAR METHODS

CONTACT FOR REAGENT AND RESOURCE SHARING

Further information and requests for resources and reagents should be directed to the lead contact, Dr. Melanie Ott, at the J. David Gladstone Institutes (melanie.ott@gladstone.ucsf.edu).

EXPERIMENTAL MODEL AND SUBJECT DETAILS

293T cells were obtained from ATCC and cultured in DMEM supplemented with 10% Fetal Bovine Serum (FBS), 1% L-glutamine, and 1% penicillin-streptomycin at 37°C, 5% CO_2. NIH3T3 cells were obtained from ATCC and cultured in DMEM supplemented with 10% Bovine Calf Serum (BCS), 1% L-glutamine, and 1% penicillin-streptomycin at 37°C, 5% CO_2.

METHOD DETAILS

Cell Fractionation and Immunoprecipitation—Cell fractionation was performed using the Dignam & Roeder method with minor modifications. 293T or NIH3T3 cells were pelleted and washed in cold DPBS. Pellets were resuspended in 5 volumes of DR Buffer A (10 mM HEPES-KOH, pH 7.9, 10 mM KCl, 1.5 mM $MgCl_2$, 0.5 mM DTT, 1x HALT, 30 nM Panobinostat and 5 μM nicotinamide). Cells were Dounce homogenized with 10 strokes using a tight pestle (Wheaton), and cytoplasmic lysates were set aside or decanted. Nuclear pellets were resuspended in DR Buffer C (20 mM HEPES, 0.42 M NaCl, 1.5 mM $MgCl_2$,

0.2 mM EDTA, 25% glycerol, 0.5 mM DTT, 1x HALT, 30 nM Panobinostat and 5 μM nicotinamide), sonicated using the Sonic Dismembrator 500 (ThermoFisher Scientific). 500 μg of nucleoplasm was precleared with normal IgG (Santa Cruz) conjugated to the appropriate beads, and immunoprecipitation was performed using anti HA-agarose beads (Sigma, A2095) or antibodies bound to Dynabeads. Immunoprecipitates were eluted either by boiling in 2x Laemmli buffer (agarose) or incubating in Elution Buffer (50 mM $NaHCO_3$, 1% SDS) and adding 2x Laemmli buffer (Dynabeads).

Lentiviral Transduction of RPRD1B shRNAs—VSV-G pseudotyped lentiviruses were produced to contain a puromycin resistance gene and a shRNA against RPRD1B (NM_027434.2–1003s21c1) or a scrambled control. Cells were transduced with 0.5 mL of unconcentrated virus and selected using 2 μg/mL puromycin for 1 week prior to experimentation.

Chromatin Immunoprecipitation in NIH3T3 Cells—NIH3T3 cells were grown under normal conditions (10% BCS, 1x penicillin and streptomycin, 2 mM L-glutamine). We treated 6×10^7 cells with a lysine deacetylase inhibitor cocktail (30 nM Panobinostat, 5 μM nicotinamide) or a vehicle control (DMSO, water) for 2 h. Cells were fixed with 1% formaldehyde for 15 min, thoroughly washed with DPBS, and resuspended in ChIP lysis buffer #1 (10 mM Tris, pH 7.4, 10 mM NaCl, 0.5% NP-40, 1x HALT, 30 nM Panobinostat and 5 μM nicotinamide). After sitting on ice for 10 min, cells were briefly vortexed, and the nuclei were pelleted. Nuclei were treated with MNase (NEB, M0247S) for 25 min at RT, pelleted and resuspended on ice in ChIP lysis buffer #2 (50 mM Tris HCl, pH 8.0, 10 mM EDTA, 0.5% SDS, 1x HALT, 30 nM Panobinostat and 5 μM nicotinamide). Chromatin was further sheared by sonication using the Sonic Dismembrator 500 (ThermoFisher Scientific) and preserved at −80°C until immunoprecipitation. 20–40 μg of chromatin was used for each IP. IPs were diluted into a final volume of 800 μL with ChIP Dilution buffer (167 mM NaCl, 16.7 mM Tris HCl, pH 8.0, 1.2 mM EDTA, 1.1% Triton X-100, 0.01% SDS) and left at 4°C overnight. IPs were washed then eluted in ChIP elution buffer (50 mM $NaHCO_3$, 1% SDS) and decrosslinked at 65°C for 16 h. Samples were treated with RNAse A (Thermofisher, EN0531) for 20 min, and DNA was purified using the QIAquick PCR purification kit (Qiagen, 28106). Primer sequences are available upon request. For samples that were deep-sequenced, 2 ng of immunoprecipitated DNA from each reaction was used to create libraries using the Ovation Ultra-Low Library prep kit (Nugen, 0344–32), following manufacturer recommendations, and libraries were deep sequenced on the HIseq 4000 or NextSeq 500 using single-end 50 bp or single-end 75 bp sequencing, respectively.

RNA Purification from NIH3T3 cells—RNA was prepared from 1×10^6 NIH3T3 cells using the QIAgen RNeasy Plus Kit. Libraries were prepared with the Ovation Ultralow System V2 kit pn: 7102–32 / 0344–32, and libraries were deep sequenced on NextSeq 500 using paired-end 75 pb sequencing.

Stable Isotope Labeling of Amino Acids in Culture (SILAC) of WT and 8KR Polymerases—SILAC labeling was performed according to the manual of SILAC Protein Quantitation Kit (LysC)–DMEM (Thermo Scientific cat. no. A33969). In brief, 293T cells stably expressing Pol-II-WT-HA and Pol-II-8KR-HA were grown in the light medium (L-Lysine-2HCl) or heavy medium ($^{13}C_6$L-Lysine-2HCl), respectively. After growing seven doubling times in the respective medium, incorporation efficiency of heavy L-lysine in 293T-Pol-II-8KR-HA cells was determined and the efficiency was more than 99%. To immunoprecipitate the HA proteins, 5 mg of total cell lysate from Pol-II-WT-HA and 5 mg of total lysate from Pol-II-8KR-HA cells in p300 lysis buffer were mixed together (total 500 μL), and 100 μL of HA agarose (Roche) were added. After overnight immunoprecipitation at 4°C, the HA-agarose was washed 4 times with 1 mL of cold p300 lysis buffer to remove

non-specific binding proteins. The bound proteins were eluted twice by 100 μL of 0.1 M glycine, pH 2.5, after a 30-min incubation. Each elution was stored in separate tube. 10 mL of 1 M Tris-HCl, pH 8.0, was added into each elution to neutralize the pH. The quality of the elution was monitored by Protein Silver Staining (Pierce). Two elusions were combined and 50 μL out of the 200 μL combined elusions were analyzed by mass spectrometry (MS). Two independent biological repeats were performed.

Samples were analyzed on a Thermo Scientific LTQ Orbitrap Elite MS system equipped with an Easy-nLC 1000 HPLC and autosampler. Samples were injected onto a pre-column (2 cm × 100 μm I.D. packed with 5 μm of C18 particles) in 100% buffer A (0.1% formic acid in water) and separated by a 120-min reverse phase gradient from 5–30% buffer B (0.1% formic acid in 100% ACN) at a flow rate of 400 nL/min. The MS continuously collected spectra in a data-dependent manner, acquiring a full scan in the Orbitrap (at 120,000 resolution with an automatic gain control target of 1,000,000 and a maximum injection time of 100 ms), followed by collision-induced dissociation spectra for the 20 most abundant ions in the ion trap (with an automatic gain control target of 10,000, a maximum injection time of 10 ms, a normalized collision energy of 35.0, activation Q of 0.250, isolation width of 2.0 m/z, and an activation time of 10.0). Singly and unassigned charge states were rejected for data-dependent selection. Dynamic exclusion was enabled to data-dependent selection of ions with a repeat count of 1, a repeat duration of 20.0 s, an exclusion duration of 20.0 s, an exclusion list size of 500, and exclusion mass width of + or - 10.00 ppm.

Isothermal Titration Calorimetry—RNA Pol II CTD peptides were purchased from Peptide 2.0 (Chantilly, VA). ITC measurements were recorded at 25 °C with a VP-ITC microcalorimeter (MicroCal). Peptides were dissolved into a buffer of 25mM Tris pH 8.0, 150 mM NaCl. 10 μL of peptide solution was injected into a sample cell containing 25 μM protein in 10mM HEPES, pH 7.5, and 150mM NaCl. A total of 25 injections were performed with a spacing of 180 s and a reference power of 15 μcal/s. Binding isotherms were plotted and analyzed with Origin Software (MicroCal). The ITC measurements were fitted to a one-site binding model (Ni et al., 2014).

Molecular Modeling—Crystallographic structures were used for the dimer (pdb:4Q94) and tetramer (pdb:4Q96) models of RPRD1B and for SCAF8 (pdb: 3D9K). Electrostatic potential surfaces were calculated using an adaptive Poisson-Boltzmann solver (APBS) from the PDB2PQR server using the Amber force field and PROPKA to assign protonation states (Dolinsky et al., 2004). Amber's LEaP program was used with the Amber ff14SB force field and the following force field modifications: phosaa10 (phosphates), ffptm (phosphorylated serines) and ALY.frcmod (acetyllysines). The TIP3P water model was used to solvate the system in a cubic periodic box, such that the closest distance between any atom in the system and the periodic boundary is 10Å. Net positive charge in the box was neutralized by adding counterions (Cl-) until neutrality. Energy minimization was performed in two steps: using harmonic restraints on the protein (10.0 kcal mol^{-1} $Å^{-2}$) and an unrestrained minimization. For each minimization, we ran 1000 steps of steepest descent and 1000 steps of conjugate-gradient minimization at a constant volume with a non-bonded cutoff of 9Å.

The equilibration was done in three steps. First, the system was heated from 0 to 300K with a restrained equilibration (10.0 kcal mol^{-1} $Å^{-2}$) for 20 ps at constant volume with a non-bonded cutoff of 9Å, using the SHAKE algorithm to constrain bonds involving hydrogens and the Andersen thermostat. The second round of equilibration was performed by lowering the harmonic restraints (1.0 kcal mol^{-1} $Å^{-2}$) on the system for 20 ps (other parameters identical). The third round was performed for 1 ns at constant pressure of 1.0 bar with non-bonded cutoff of 9Å at 300K with the Andersen thermostat. Simulations were performed without restraints using new velocities with random seeds at constant pressure of 1 bar with non-bonded cutoff distance of 9Å. 20-ns simulations were run with 2 fs timesteps per construct. Coordinates and energy were saved every picosecond (500 steps) (Case et al., 2005). Molecular graphics and analyses were performed with the UCSF Chimera package (Pettersen et al., 2004).

QUANTIFICATION AND STATISTICAL ANALYSIS

MS Analysis—Raw MS data were analyzed using the MaxQuant software package (version 1.2.5.8) (Cox and Mann, 2008). Data were matched to the SwissProt human proteins (downloaded from UniProt on 2/15/13, 20,259 protein sequence entries). MaxQuant was configured to generate and search against a reverse sequence database for false discovery rate calculations. Variable modifications were allowed for methionine oxidation and protein N-terminus acetylation. A fixed modification was indicated for cysteine carbamidomethylation. Full trypsin specificity was required. The first search was performed with a mass accuracy of +/− 20 parts per million, and the main search was performed with a mass accuracy of +/− 6 parts per million. A maximum of five modifications were allowed per peptide. A maximum of two missed cleavages were allowed. The maximum charge allowed was 7+. Individual peptide mass tolerances were allowed. For MS/MS matching, a mass tolerance of 0.5 Da was allowed and the top six peaks per 100 Da were analyzed. MS/MS matching was allowed for higher charge states, water and ammonia loss events. The data were filtered to obtain peptide, protein, and site-level false discovery rates of 0.01. The minimum peptide length was seven amino acids. Results were matched between runs with a time window of 2 min for technical duplicates.

Western Blots—Quantification of western blots was done with ImageJ. P-values were determined using a one-sided T-test.

RNA Sequencing—RNA-seq analysis and statistical calculations were done using the Illumina RNAexpress application v 1.1.0.

ChIP-seq Data Analysis—Barcodes were removed and sequences were trimmed using Skewer version 0.1.124 (Jiang et al., 2014). For each ChIP 50–60 million reads were aligned to the *Mus musculus* mm10 genome assembly using Bowtie version 1.1.2 with the –a -l 55 -n 2 -m 1 parameter (Langmead et al., 2009). Peaks were called and sequence pileups normalized to reads per million relative to input controls using MACS2 version 2.1.0.20150731 using the following parameters -B -SPMR -g mm -no-model -slocal 1000 (Zhang et al., 2008). TSS profiling was done using plotProfile on matrices generated with 10-bp bins using the computeMatrix function found in the Deeptools version 2.2.3 (Ramirez

et al., 2016). Reproducibility of data was assessed by principal component analysis using the plotPCA function (Ramirez et al., 2016).

DATA AND SOFWARE AVAILABILITY

ChIP-seq data was deposited into GEO under the accession number GSE124996. RNA-seq data was deposited into GEO under the accession number GSE125486. Western Blotting and Structural Modeling Data were deposited into Mendeley Data under the doi 10.17632/f6w4wzb9dr.1.

Supplementary Material

Refer to Web version on PubMed Central for supplementary material.

ACKNOWLEDGEMENTS

We thank members of the Ott laboratory, J.J. Miranda, PhD, and Bassem Al Sady, PhD, for helpful discussions, reagents and expertise. Natasha Carli, PhD, and Jim McGuire from the Gladstone Genomics Core for library preparation and QCs for next-generation sequencing and for funding from the James B. Pendleton Charitable Trust. We are grateful for funding support from the NIH R01AI083139 (M.O.), P50-GM082250 (N.J.K.), and P01-CA177322 (J.R.J) UCSF Discovery Fellowship and American Society for Microbiology, Robert D. Watkins Graduate Research Fellowship (I.A.), and funding from the NSERC RGPIN-2016–06300 (J.M.). We thank John Carroll for graphics, Kathryn Claiborn and Gary Howard for editing and Lauren Weiser for administrative support. Chimera is developed by the Resource for Biocomputing, Visualization, and Informatics at the University of California, San Francisco (supported by NIGMS P41-GM103311).

REFERENCES

BARTKOWIAK B, LIU P, PHATNANI HP, FUDA NJ, COOPER JJ, PRICE DH, ADELMAN K, LIS JT & GREENLEAF AL 2010 CDK12 is a transcription elongation-associated CTD kinase, the metazoan ortholog of yeast Ctk1. Genes Dev, 24, 2303–16. [PubMed: 20952539]

BARTOLOMEI MS & CORDEN JL 1987 Localization of an alpha-amanitin resistance mutation in the gene encoding the largest subunit of mouse RNA polymerase II. Mol Cell Biol, 7, 586–94. [PubMed: 3821724]

BASTA J & RAUCHMAN M 2015 The nucleosome remodeling and deacetylase complex in development and disease. Transl Res, 165, 36–47. [PubMed: 24880148]

BECKER R, LOLL B & MEINHART A 2008 Snapshots of the RNA processing factor SCAF8 bound to different phosphorylated forms of the carboxyl-terminal domain of RNA polymerase II. J Biol Chem, 283, 22659–69. [PubMed: 18550522]

BROOKES E, DE SANTIAGO I, HEBENSTREIT D, MORRIS KJ, CARROLL T, XIE SQ, STOCK JK, HEIDEMANN M, EICK D, NOZAKI N, KIMURA H, RAGOUSSIS J, TEICHMANN SA & POMBO A 2012 Polycomb associates genome-wide with a specific RNA polymerase II variant, and regulates metabolic genes in ESCs. Cell Stem Cell, 10, 157–70. [PubMed: 22305566]

BURATOWSKI S 2003 The CTD code. Nat Struct Biol, 10, 679–80. [PubMed: 12942140]

BURATOWSKI S 2009 Progression through the RNA polymerase II CTD cycle. Mol Cell, 36, 541–6. [PubMed: 19941815]

CASE DA, CHEATHAM TE 3RD, DARDEN T, GOHLKE H, LUO R, MERZ KM JR., ONUFRIEV A, SIMMERLING C, WANG B & WOODS RJ 2005 The Amber biomolecular simulation programs. J Comput Chem, 26, 1668–88. [PubMed: 16200636]

CHAPMAN RD, HEIDEMANN M, HINTERMAIR C & EICK D 2008 Molecular evolution of the RNA polymerase II CTD. Trends Genet, 24, 289–96. [PubMed: 18472177]

COX J & MANN M 2008 MaxQuant enables high peptide identification rates, individualized p.p.b.-range mass accuracies and proteome-wide protein quantification. Nat Biotechnol, 26, 1367–72. [PubMed: 19029910]

DESCOSTES N, HEIDEMANN M, SPINELLI L, SCHULLER R, MAQBOOL MA, FENOUIL R, KOCH F, INNOCENTI C, GUT M, GUT I, EICK D & ANDRAU JC 2014 Tyrosine phosphorylation of RNA polymerase II CTD is associated with antisense promoter transcription and active enhancers in mammalian cells. Elife, 3, e02105. [PubMed: 24842994]

DEVAIAH BN, LEWIS BA, CHERMAN N, HEWITT MC, ALBRECHT BK, ROBEY PG, OZATO K, SIMS RJ 3RD & SINGER DS 2012 BRD4 is an atypical kinase that phosphorylates serine2 of the RNA polymerase II carboxy-terminal domain. Proc Natl Acad Sci U S A, 109, 6927–32. [PubMed: 22509028]

DIAS JD, RITO T, TORLAI TRIGLIA E, KUKALEV A, FERRAI C, CHOTALIA M, BROOKES E, KIMURA H & POMBO A 2015 Methylation of RNA polymerase II non-consensus Lysine residues marks early transcription in mammalian cells. Elife, 4.

DOLINSKY TJ, NIELSEN JE, MCCAMMON JA & BAKER NA 2004 PDB2PQR: an automated pipeline for the setup of Poisson-Boltzmann electrostatics calculations. Nucleic Acids Res, 32, W665–7. [PubMed: 15215472]

EBMEIER CC, ERICKSON B, ALLEN BL, ALLEN MA, KIM H, FONG N, JACOBSEN JR, LIANG K, SHILATIFARD A, DOWELL RD, OLD WM, BENTLEY DL & TAATJES DJ 2017 Human TFIIH Kinase CDK7 Regulates Transcription-Associated Chromatin Modifications. Cell Rep, 20, 1173–1186. [PubMed: 28768201]

EGLOFF S, ZABOROWSKA J, LAITEM C, KISS T & MURPHY S 2012 Ser7 phosphorylation of the CTD recruits the RPAP2 Ser5 phosphatase to snRNA genes. Mol Cell, 45, 111–22. [PubMed: 22137580]

EICK D & GEYER M 2013 The RNA polymerase II carboxy-terminal domain (CTD) code. Chem Rev, 113, 8456–90. [PubMed: 23952966]

HARLEN KM & CHURCHMAN LS 2017 The code and beyond: transcription regulation by the RNA polymerase II carboxy-terminal domain. Nat Rev Mol Cell Biol, 18, 263–273. [PubMed: 28248323]

HEIDEMANN M, HINTERMAIR C, VOSS K & EICK D 2013 Dynamic phosphorylation patterns of RNA polymerase II CTD during transcription. Biochim Biophys Acta, 1829, 55–62. [PubMed: 22982363]

HINTERMAIR C, HEIDEMANN M, KOCH F, DESCOSTES N, GUT M, GUT I, FENOUIL R, FERRIER P, FLATLEY A, KREMMER E, CHAPMAN RD, ANDRAU JC & EICK D 2012 Threonine-4 of mammalian RNA polymerase II CTD is targeted by Polo-like kinase 3 and required for transcriptional elongation. EMBO J, 31, 2784–97. [PubMed: 22549466]

HSIN JP & MANLEY JL 2012 The RNA polymerase II CTD coordinates transcription and RNA processing. Genes Dev, 26, 2119–37. [PubMed: 23028141]

JASNOVIDOVA O, KLUMPLER T, KUBICEK K, KALYNYCH S, PLEVKA P & STEFL R 2017 Structure and dynamics of the RNAPII CTDsome with Rtt103. Proc Natl Acad Sci U S A, 114, 11133–11138. [PubMed: 29073019]

JASNOVIDOVA O & STEFL R 2013 The CTD code of RNA polymerase II: a structural view. Wiley Interdiscip Rev RNA, 4, 1–16. [PubMed: 23042580]

JIANG H, LEI R, DING SW & ZHU S 2014 Skewer: a fast and accurate adapter trimmer for next-generation sequencing paired-end reads. BMC Bioinformatics, 15, 182. [PubMed: 24925680]

JIN K, CHEN H, ZUO Q, HUANG C, ZHAO R, YU X, WANG Y, ZHANG Y, CHANG Z & LI B 2018 CREPT and p15RS regulate cell proliferation and cycling in chicken DF-1 cells through the Wnt/beta-catenin pathway. J Cell Biochem, 119, 1083–1092. [PubMed: 28695988]

LANGMEAD B, TRAPNELL C, POP M & SALZBERG SL 2009 Ultrafast and memory-efficient alignment of short DNA sequences to the human genome. Genome Biol, 10, R25. [PubMed: 19261174]

LIU C, ZHANG Y, LI J, WANG Y, REN F, ZHOU Y, WU Y, FENG Y, ZHOU Y, SU F, JIA B, WANG D & CHANG Z 2015 p15RS/RPRD1A (p15INK4b-related sequence/regulation of nuclear pre-mRNA domain-containing protein 1A) interacts with HDAC2 in inhibition of the Wnt/beta-catenin signaling pathway. J Biol Chem, 290, 9701–13. [PubMed: 25697359]

LIU J, LIU H, ZHANG X, GAO P, WANG J & HU Z 2002 Identification and characterization of P15RS, a novel P15(INK4b) related gene on G1/S progression. Biochem Biophys Res Commun, 299, 880–5. [PubMed: 12470661]

LU D, WU Y, WANG Y, REN F, WANG D, SU F, ZHANG Y, YANG X, JIN G, HAO X, HE D, ZHAI Y, IRWIN DM, HU J, SUNG JJ, YU J, JIA B & CHANG Z 2012 CREPT accelerates tumorigenesis by regulating the transcription of cell-cycle-related genes. Cancer Cell, 21, 92–104. [PubMed: 22264791]

MEI K, JIN Z, REN F, WANG Y, CHANG Z & WANG X 2014 Structural basis for the recognition of RNA polymerase II C-terminal domain by CREPT and p15RS. Sci China Life Sci, 57, 97–106. [PubMed: 24399136]

MEINHART A & CRAMER P 2004 Recognition of RNA polymerase II carboxy-terminal domain by 3'-RNA-processing factors. Nature, 430, 223–6. [PubMed: 15241417]

MORALES JC, RICHARD P, ROMMEL A, FATTAH FJ, MOTEA EA, PATIDAR PL, XIAO L, LESKOV K, WU SY, HITTELMAN WN, CHIANG CM, MANLEY JL & BOOTHMAN DA 2014 Kub5-Hera, the human Rtt103 homolog, plays dual functional roles in transcription termination and DNA repair. Nucleic Acids Res, 42, 4996–5006. [PubMed: 24589584]

MULLER S, FILIPPAKOPOULOS P & KNAPP S 2011 Bromodomains as therapeutic targets. Expert Rev Mol Med, 13, e29. [PubMed: 21933453]

NECHAEV S & ADELMAN K 2011 Pol II waiting in the starting gates: Regulating the transition from transcription initiation into productive elongation. Biochim Biophys Acta, 1809, 34–45. [PubMed: 21081187]

NI Z, OLSEN JB, GUO X, ZHONG G, RUAN ED, MARCON E, YOUNG P, GUO H, LI J, MOFFAT J, EMILI A & GREENBLATT JF 2011 Control of the RNA polymerase II phosphorylation state in promoter regions by CTD interaction domain-containing proteins RPRD1A and RPRD1B. Transcription, 2, 237–42. [PubMed: 22231121]

NI Z, XU C, GUO X, HUNTER GO, KUZNETSOVA OV, TEMPEL W, MARCON E, ZHONG G, GUO H, KUO WW, LI J, YOUNG P, OLSEN JB, WAN C, LOPPNAU P, EL BAKKOURI M, SENISTERRA GA, HE H, HUANG H, SIDHU SS, EMILI A, MURPHY S, MOSLEY AL, ARROWSMITH CH, MIN J & GREENBLATT JF 2014 RPRD1A and RPRD1B are human RNA polymerase II C-terminal domain scaffolds for Ser5 dephosphorylation. Nat Struct Mol Biol, 21, 686–695. [PubMed: 24997600]

PATIDAR PL, MOTEA EA, FATTAH FJ, ZHOU Y, MORALES JC, XIE Y, GARNER HR & BOOTHMAN DA 2016 The Kub5-Hera/RPRD1B interactome: a novel role in preserving genetic stability by regulating DNA mismatch repair. Nucleic Acids Res, 44, 1718–31. [PubMed: 26819409]

PATTURAJAN M, WEI X, BEREZNEY R & CORDEN JL 1998 A nuclear matrix protein interacts with the phosphorylated C-terminal domain of RNA polymerase II. Mol Cell Biol, 18, 2406–15. [PubMed: 9528809]

PERUTZ MF, JOHNSON T, SUZUKI M & FINCH JT 1994 Glutamine repeats as polar zippers: their possible role in inherited neurodegenerative diseases. Proc Natl Acad Sci U S A, 91, 5355–8. [PubMed: 8202492]

PETTERSEN EF, GODDARD TD, HUANG CC, COUCH GS, GREENBLATT DM, MENG EC & FERRIN TE 2004 UCSF Chimera--a visualization system for exploratory research and analysis. J Comput Chem, 25, 1605–12. [PubMed: 15264254]

PINEDA G, SHEN Z, DE ALBUQUERQUE CP, REYNOSO E, CHEN J, TU CC, TANG W, BRIGGS S, ZHOU H & WANG JY 2015 Proteomics studies of the interactome of RNA polymerase II C-terminal repeated domain. BMC Res Notes, 8, 616. [PubMed: 26515650]

RAMIREZ F, RYAN DP, GRUNING B, BHARDWAJ V, KILPERT F, RICHTER AS, HEYNE S, DUNDAR F & MANKE T 2016 deepTools2: a next generation web server for deep-sequencing data analysis. Nucleic Acids Res, 44, W160–5. [PubMed: 27079975]

SCHRODER S, HERKER E, ITZEN F, HE D, THOMAS S, GILCHRIST DA, KAEHLCKE K, CHO S, POLLARD KS, CAPRA JA, SCHNOLZER M, COLE PA, GEYER M, BRUNEAU BG, ADELMAN K & OTT M 2013 Acetylation of RNA polymerase II regulates growth-factor-induced gene transcription in mammalian cells. Mol Cell, 52, 314–24. [PubMed: 24207025]

SCHULLER R, FORNE I, STRAUB T, SCHREIECK A, TEXIER Y, SHAH N, DECKER TM, CRAMER P, IMHOF A & EICK D 2016 Heptad-Specific Phosphorylation of RNA Polymerase II CTD. Mol Cell, 61, 305–14. [PubMed: 26799765]

SHAH N, MAQBOOL MA, YAHIA Y, EL AABIDINE AZ, ESNAULT C, FORNE I, DECKER TM, MARTIN D, SCHULLER R, KREBS S, BLUM H, IMHOF A, EICK D & ANDRAU JC 2018 Tyrosine-1 of RNA Polymerase II CTD Controls Global Termination of Gene Transcription in Mammals. Mol Cell, 69, 48–61 e6. [PubMed: 29304333]

SIMONTI CN, POLLARD KS, SCHRODER S, HE D, BRUNEAU BG, OTT M & CAPRA JA 2015 Evolution of lysine acetylation in the RNA polymerase II C-terminal domain. BMC Evol Biol, 15, 35. [PubMed: 25887984]

SIMS RJ 3RD, ROJAS LA, BECK DB, BONASIO R, SCHULLER R, DRURY WJ 3RD, EICK D & REINBERG D 2011 The C-terminal domain of RNA polymerase II is modified by site-specific methylation. Science, 332, 99–103. [PubMed: 21454787]

SUH H, FICARRO SB, KANG UB, CHUN Y, MARTO JA & BURATOWSKI S 2016 Direct Analysis of Phosphorylation Sites on the Rpb1 C-Terminal Domain of RNA Polymerase II. Mol Cell, 61, 297–304. [PubMed: 26799764]

TSAI PF, DELL'ORSO S, RODRIGUEZ J, VIVANCO KO, KO KD, JIANG K, JUAN AH, SARSHAD AA, VIAN L, TRAN M, WANGSA D, WANG AH, PEROVANOVIC J, ANASTASAKIS D, RALSTON E, RIED T, SUN HW, HAFNER M, LARSON DR & SARTORELLI V 2018 A Muscle-Specific Enhancer RNA Mediates Cohesin Recruitment and Regulates Transcription In trans. Mol Cell, 71, 129–141 e8. [PubMed: 29979962]

VIAN L, PEKOWSKA A, RAO SSP, KIEFFER-KWON KR, JUNG S, BARANELLO L, HUANG SC, EL KHATTABI L, DOSE M, PRUETT N, SANBORN AL, CANELA A, MAMAN Y, OKSANEN A, RESCH W, LI X, LEE B, KOVALCHUK AL, TANG Z, NELSON S, DI PIERRO M, CHENG RR, MACHOL I, ST HILAIRE BG, DURAND NC, SHAMIM MS, STAMENOVA EK, ONUCHIC JN, RUAN Y, NUSSENZWEIG A, LEVENS D, AIDEN EL & CASELLAS R 2018 The Energetics and Physiological Impact of Cohesin Extrusion. Cell, 173, 1165–1178 e20. [PubMed: 29706548]

VOSS K, FORNE I, DESCOSTES N, HINTERMAIR C, SCHULLER R, MAQBOOL MA, HEIDEMANN M, FLATLEY A, IMHOF A, GUT M, GUT I, KREMMER E, ANDRAU JC & EICK D 2015 Site-specific methylation and acetylation of lysine residues in the C-terminal domain (CTD) of RNA polymerase II. Transcription, 6, 91–101. [PubMed: 26566685]

WEINERT BT, NARITA T, SATPATHY S, SRINIVASAN B, HANSEN BK, SCHOLZ C, HAMILTON WB, ZUCCONI BE, WANG WW, LIU WR, BRICKMAN JM, KESICKI EA, LAI A, BROMBERG KD, COLE PA & CHOUDHARY C 2018 Time-Resolved Analysis Reveals Rapid Dynamics and Broad Scope of the CBP/p300 Acetylome. Cell, 174, 231–244 e12. [PubMed: 29804834]

WU Y, ZHANG Y, ZHANG H, YANG X, WANG Y, REN F, LIU H, ZHAI Y, JIA B, YU J & CHANG Z 2010 p15RS attenuates Wnt/{beta}-catenin signaling by disrupting {beta}-catenin.TCF4 Interaction. J Biol Chem, 285, 34621–31. [PubMed: 20739273]

XUE Y, WONG J, MORENO GT, YOUNG MK, COTE J & WANG W 1998 NURD, a novel complex with both ATP-dependent chromatin-remodeling and histone deacetylase activities. Mol Cell, 2, 851–61. [PubMed: 9885572]

YURKO NM & MANLEY JL 2018 The RNA polymerase II CTD "orphan" residues: Emerging insights into the functions of Tyr-1, Thr-4, and Ser-7. Transcription, 9, 30–40. [PubMed: 28771071]

ZABOROWSKA J, EGLOFF S & MURPHY S 2016 The pol II CTD: new twists in the tail. Nat Struct Mol Biol, 23, 771–7. [PubMed: 27605205]

ZHANG Y, LIU T, MEYER CA, EECKHOUTE J, JOHNSON DS, BERNSTEIN BE, NUSBAUM C, MYERS RM, BROWN M, LI W & LIU XS 2008 Model-based analysis of ChIP-Seq (MACS). Genome Biol, 9, R137. [PubMed: 18798982]

ZHANG Y, WANG S, KANG W, LIU C, DONG Y, REN F, WANG Y, ZHANG J, WANG G, TO KF, ZHANG X, SUNG JJ, CHANG Z & YU J 2018 CREPT facilitates colorectal cancer growth through inducing Wnt/beta-catenin pathway by enhancing p300-mediated beta-catenin acetylation. Oncogene, 37, 3485–3500. [PubMed: 29563608]

Highlights

- RPRD proteins interact with the RNA Pol II CTD in an acetylation-dependent manner
- RPRD CTD-interacting domain amide residues stabilize acetylated CTD heptads
- KDAC inhibition enahnces Pol II CTD K7-acetylation & reduces S5-phosphorylation
- RPRD1B knockdown disrupts Pol II CTD deacetylase & CTD phosphatase activity

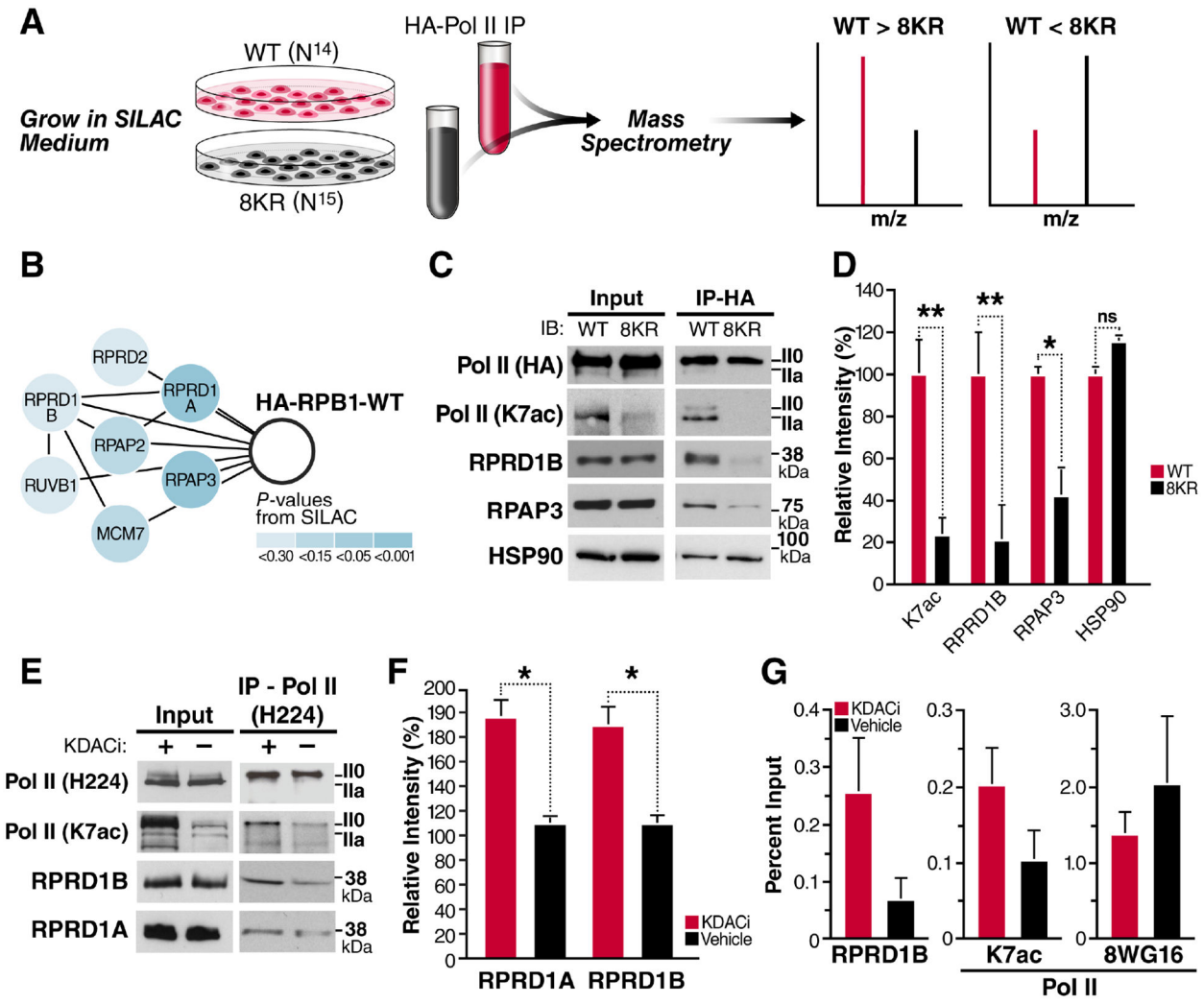

Figure 1: RPRD Proteins Interact with RPB1 in an Acetylation-Dependent Manner.

(A) A SILAC-based mass spectrometry screen was used to identify factors that bind preferentially to WT Pol II, compared to the 8KR mutant.

(B) Components of the RPRD1B/RPRD1A complex that were identified as WT interactors.

(C) Hemagglutinin (HA) immunoprecipitation and western blotting with the indicated antibodies RPRD1B or from WT and 8KR cells.

(D) Densitometry using ImageJ of at least three independent western blots from indicated antibodies after HA-immunoprecipitation.

(E) NIH3T3 cells were treated with KDAC inhibitors (30 nM Panobinostat and 5 μM Nicotinamide) for 2 h. IP using an N-terminal H224 antibody from 500 μg of nucleoplasm pre-cleared with IgG and western blotting with the indicated antibodies.

(F) Densitometry of RPRD1A and RPRD1B western blots produced from three independent Pol II Total (H224) IP elutions.

(G) ChIP-qPCR on the *Leo1* gene at +33 nt downstream of TSS using the indicated antibodies from 4 independent chromatin preparations. Unmodified Pol II ChIP experiments

were done with the 8WG16 antibody. Values are represented as percent of input with IgG subtracted.

Data is shown as mean ± SEM. *p < 0.5; **p < 0.01; ns, not significant for a one-tailed T test. See also Table S1.

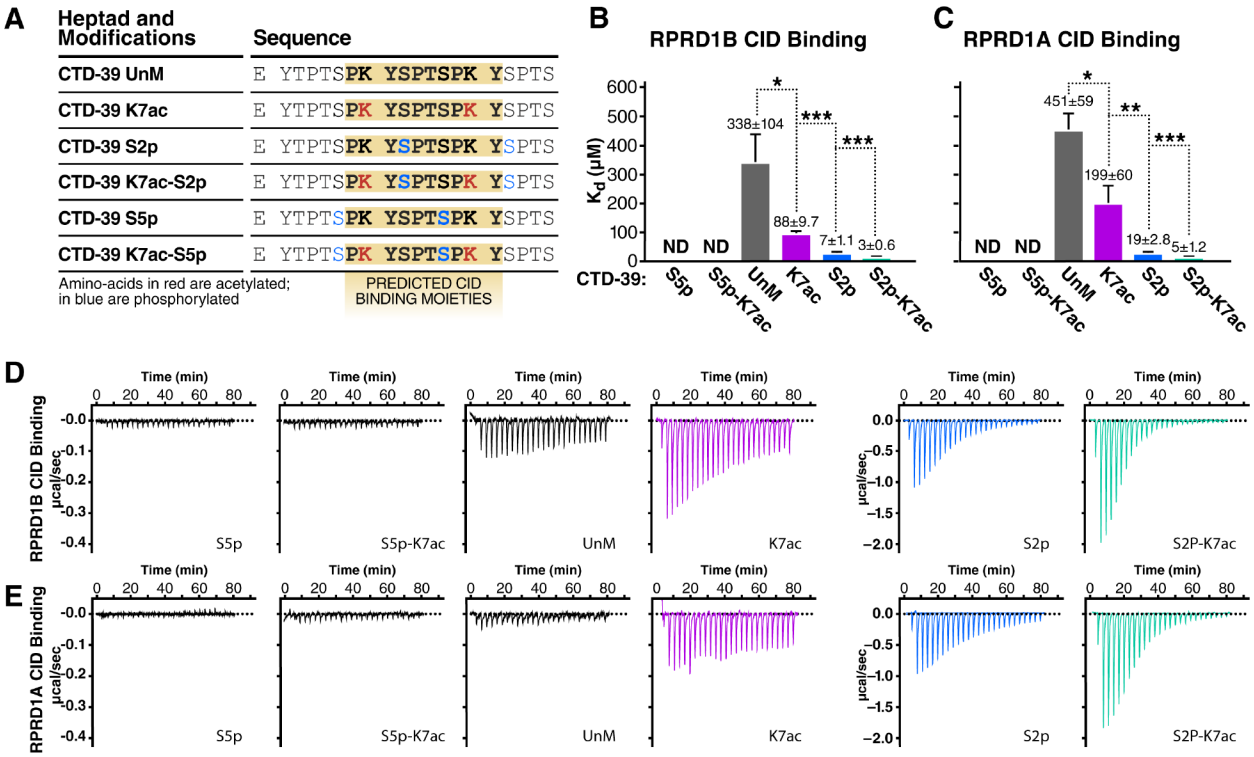

Figure 2: RPRD CID Domains Recognize Acetylated and Phosphorylated CTD Peptides.

Isothermal titration calorimetry (ITC) experiments measuring *in-vitro* binding affinity between RPRD1A and RPRD1B CID domains and modified CTD peptides.

(A) Table of CTD-39 peptides with indicated post-translational modifications and predicted RPRD CID binding moieties.

(B) K_d values measured by ITC for RPRD1B CID and modified CTD-39 binding.

(C) K_d values measured by ITC for RPRD1A CID and modified CTD-39 binding.

(D) Representative ITC plots showing effect of K7ac on RPRD1B CID-CTD interactions for the indicated modifications

(E) Representative ITC plots showing effect of K7ac on RPRD1A CID-CTD interactions for the indicated modifications.

Data is shown as mean ± SEM. * $p < 0.05$; ** $p < 0.01$; *** $p < 0.005$ using a one-tailed T test.

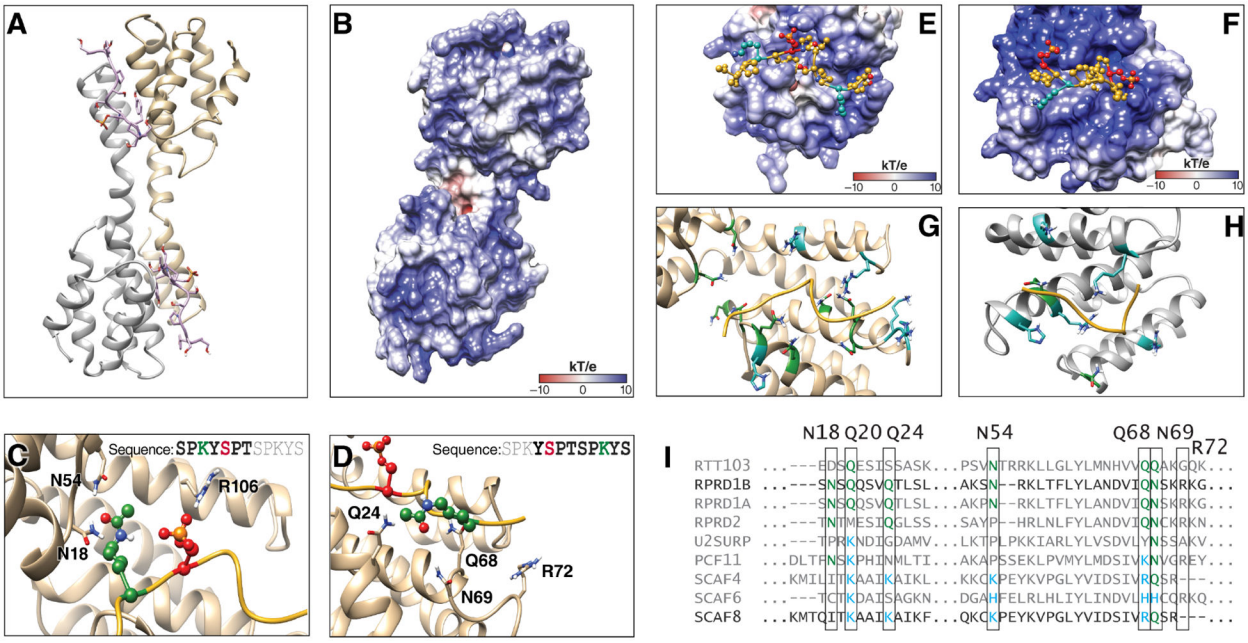

Figure 3: Molecular Modeling of K7 Acetylation and Interaction with CID Domains.

(A) Dimer model from RPRD1B crystal structure (pdb:4Q94) containing two recognition modules and two peptides fragments of the CTD.

(B) Electrostatic potential surface for RPRD1B CID.

(C) Recognition elements around first K7ac and S2p in the CTD peptide fragment.

(D) Recognition elements around second K7ac in the CTD peptide fragment.

(E) CTD peptide fragment model from crystal structure superimposed with the electrostatic surface potential around the corresponding binding site.

(F) CTD peptide fragment superimposed with the electrostatic potential surface around the corresponding SCAF8 CID binding site

(G) RPRD1B CID residues found within 5Å of peptide fragment. Blue: positively charged residues. Green: amide-containing residues.

(H) SCAF8 CID residues found within 5Å of peptide fragment. Blue: positively charged residues. Green: amide-containing residues.

(I) Clustal Omega sequence alignment of human CID regions with yeast RTT103 as outgroup. Green: amide-containing residues. Blue: positively charged residues. See also Figure S1.

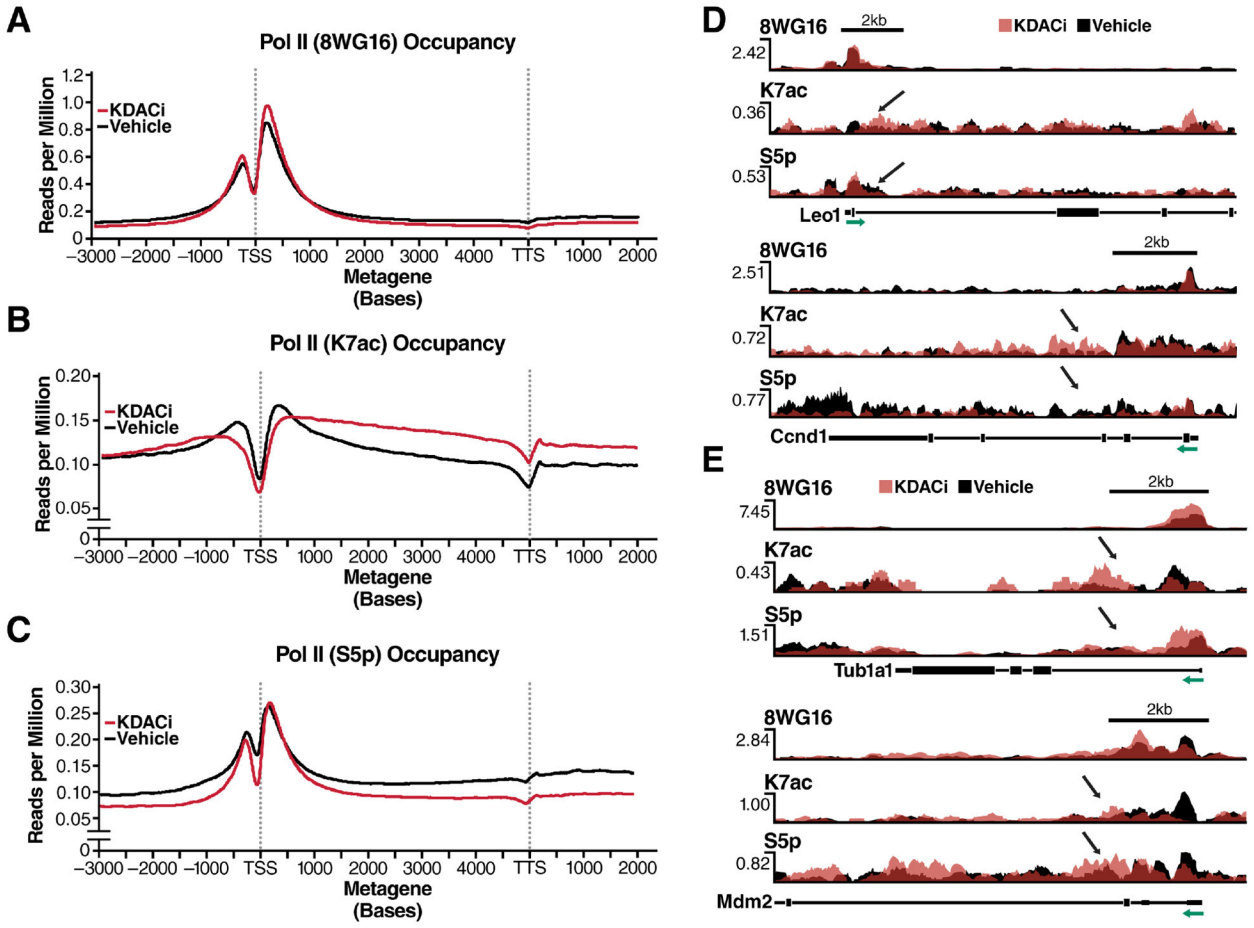

Figure 4: An Inverse Relationship between K7ac and Phosphorylation Is Induced upon KDAC Inhibition.

(A-C) Metagene profiles generated from chromatin immunoprecipitation experiments in NIH3T3 cells with the indicated antibodies followed by deep-sequencing. Gene profiles are measured in reads per million normalized to input control

(D) Single-gene validation of RNA Pol II PTMs measured as reads per million on selected RPRD1B occupied genes. S5p was measured using the RNA Pol II 4H8 antibody.

(E) Occupancy profiles of RNA Pol II PTMs on control genes. Green arrows indicate the direction of transcription relative to the TSS of the depicted gene. Black arrows indicate the site of affected PTMs in response to KDACi.

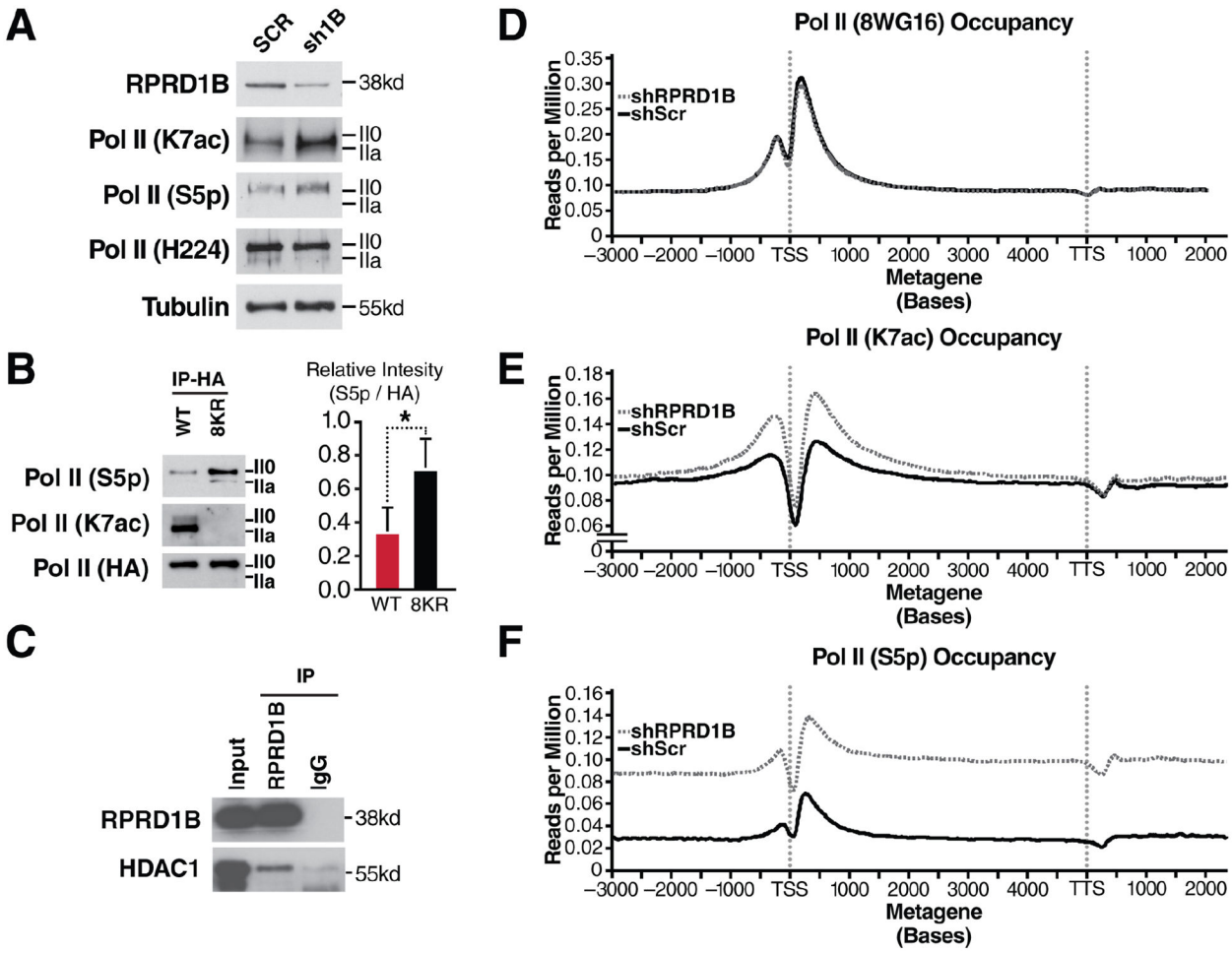

Figure 5: Increased S5p and K7ac Levels in Response to RPRD1B Knockdown.

(A) Western blotting of indicated RNA Pol II modifications in NIH3T3 cells treated with scrambled shRNAs or those targeting RPRD1B.

(B) Western blotting against S5p and K7ac from HA-immunopurified lysates containing WT or 8KR RNA Pol II and densitometry using ImageJ of three independent HA-elutions.

(C) RPRD1B immunoprecipitation from 293T cell lysates and western blotting against nuclear histone deacetylase HDAC1.

(D-F) Metagene profiles of expressed genes in NIH3T3 cells. Gene profiles are measured in reads per million, relative to input control. Metagene profiles were generated from ChIP-seq data from NIH3T3 cells expressing either scrambled or RPRD1B targeted shRNAs treated with vehicle control. S5p is measured using the RNA Pol II 4H8 antibody. Profiles are representative of two independent experiments.

Data is shown as mean ± SEM. * $p < 0.05$; using a one-tailed T test. See also Figure S2 and Table S2.

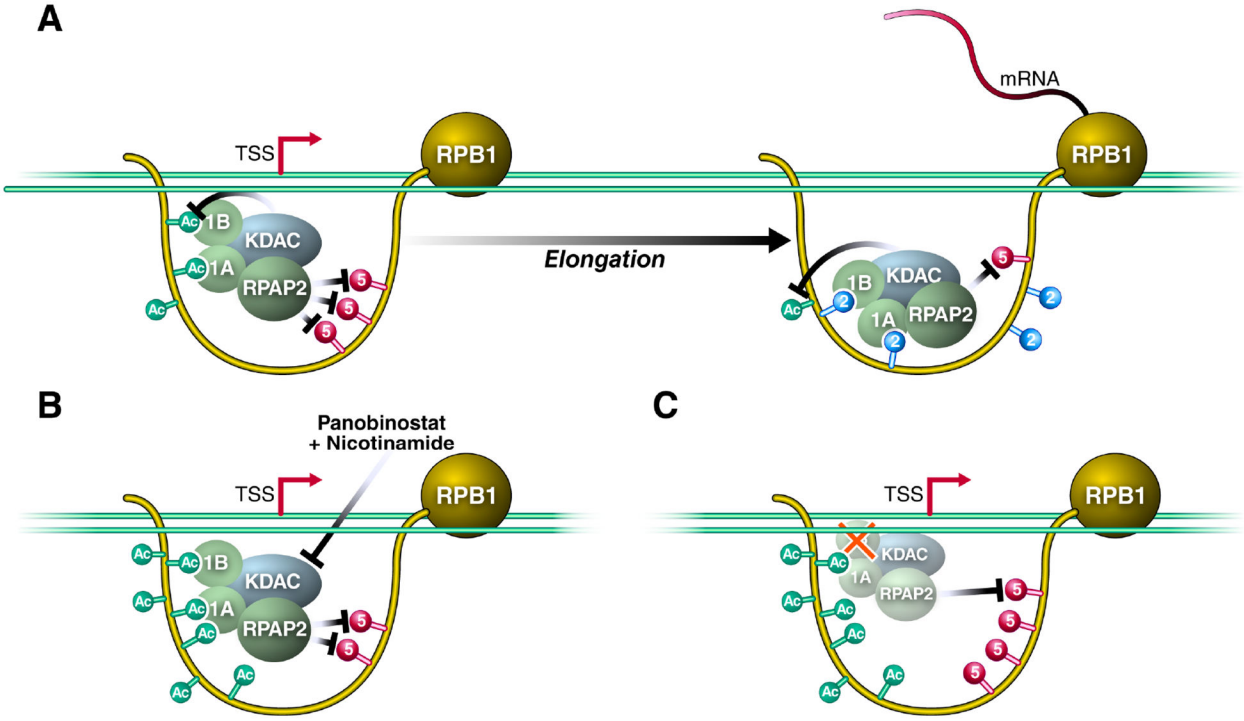

Figure 6: RPRD Proteins Are Recruited to the RPB1 CTD via Acetylation and Phosphorylation to Antagonize S5-Phosphorylation.

(A) Model of RPRD complex reader and effector functions along modified residues within the CTD. 1B- RPRD1B 1A- RPRD1A, KDAC represents RPRD associated K7 deacetylases.

(B) KDAC inhibition induces K7 hyperacetylation and downregulation of S5-phosphorylation.

(C) Knockdown of RPRD1B perturbs the recruitment of the complex to result in both S5 hyperphosphorylation and K7 hyperacetylation. See text for details.

KEY RESOURCES TABLE

REAGENT or RESOURCE	SOURCE	IDENTIFIER
Antibodies		
RPRD1B (Rabbit)	Bethyl	AB_11218400
RPRD1B (Mouse)	Novus	AB_2285416
RRPD1A	Santa Cruz	sc514724
Pol II (8WG16)	Abcam	AB_306327
Pol II (4H8)	Abcam	AB_304868
Pol II (H224)	Santa Cruz	AB_2268548
Pol II (K7ac)	This Paper	N/A
RPAP3	Bethyl	AB_2621049
HA (Rat)	Sigma	AB_10094468
HA Agarose Bead	Sigma	AB_257974
HA Magnetic Bead	Sigma	AB_2749815
Normal IgG (Rabbit)	Santa Cruz	AB_737197
Normal IgG (Mouse)	Santa Cruz	AB_737182
HSP90	Abcam	AB_444729
HDAC1	Abcam	AB_2264059
AffiniPure Goat Anti-Mouse HRP	Jackson Immunoresearch	AB_10015289
AffiniPure Goat Anti-Rabbit HRP	Jackson Immunoresearch	AB_2313567
AffiniPure Goat Anti-Rat HRP	Jackson Immunoresearch	AB_2338128
Chemicals, Peptides, and Recombinant Proteins		
Panobinostat	Santa Cruz	CAS 404950-80-7
Nicotinamide	Sigma	CAS 98-92-0
α-Amanitin	Santa Cruz	CAS 23109-05-9
CTD Peptides	Peptide 2.0	N/A
Critical Commercial Assays		
QIAquick PCR Purification Kit	Qiagen	28104
RNeasy Plus Mini Kit	Qiagen	74136
Ovation Ultralow System V2	NuGEN	0344-32
Deposited Data		
RNA Pol II ChIP-seq Data	GEO	GSE124996
RNA Seq Data	GEO	GSE125486
Western Blotting Data	Mendeley Data	DOI: 10.17632/f6w4wzb9dr.1
Structural Modeling	Mendeley Data	DOI: 10.17632/f6w4wzb9dr.1
SILAC Data	This Paper	Table S1

REAGENT or RESOURCE	SOURCE	IDENTIFIER
Experimental Models: Cell Lines		
NIH3T3	ATCC	CRL-1658
293T	ATCC	CRL-3216
Software and Algorithms		
Skewer v 0.1.124	Jiang et al., 2014	N/A
Bowtie v 1.1.2	Langmead et al., 2009	N/A
MACS2 v 2.1.0.20150731	Zhang et al., 2008	N/A
DeepTools v 2.2.3	Ramirez et al., 2016	N/A
MaxQuant v 1.2.5.8	Cox and Mann, 2008	N/A